Synthesis and Characterization of New Five-Coordinate Platinum Nitrosyl Derivatives: Density Functional Theory Study of Their Electronic Structure

Irene Ara,[a] Juan Forniés,*[a] María Angeles García-Monforte,[a] Babil Menjón,[a] Rosa María Sanz-Carrillo,[a] Milagros Tomás,[a] Athanassios C. Tsipis,[b] and Constantinos A. Tsipis*[b]

Abstract: The neutral, five-coordinate platinum nitrosyl compounds $[Pt(C_6F_5)_3(L)(NO)]$ (**2**) [L = CN*t*Bu (**2a**), NC_5H_4Me-4 (**2b**), $PPhMe_2$ (**2c**), PPh_3 (**2d**) and tht (**2e**)] have been prepared by the reaction of $[NBu_4][Pt(C_6F_5)_3(L)]$ (**1**) with $NOClO_4$ in CH_2Cl_2. The ionic compound $[N(PPh_3)_2][Pt(C_6F_5)_4(NO)]$ (**4**) has been prepared in a similar way starting from the homoleptic species $[N(PPh_3)_2]_2$-$[Pt(C_6F_5)_4]$ (**3**). Compounds **2** and **4** are all diamagnetic with $\{PtNO\}^8$ electronic configuration and show ν(NO) stretching frequencies at around 1800 cm^{-1}. The crystal and molecular structures of **2c** and **4** have been established by X-ray diffraction methods. The coordination environment for the Pt center in both compounds can be described as square pyramidal (*SPY*-5). Bent nitrosyl coordination is observed in both cases with Pt-N-O angles of 120.1(6) and 130.2(7)° for **2c** and **4**, respectively. The bonding mechanism of the nitrosyl ligand coordinated to various model $[Pt^{II}R_4]^{2-}$ (R = H, Me, Cl, CN, C_6F_5 or C_6Cl_5) and $[Pt(C_6F_5)_3(L)]^-$ (L = CNMe, PH_3) systems has been studied by density functional calculations at the B3LYP level of theory, using the SDD basis set. The R_4Pt–NO and $(C_6F_5)_3(L)Pt$–NO interactions generally involve two components: i) a direct Pt–NO bonding interaction and ii) multicenter-bonding interactions between the N atom of the NO ligand and the donor atoms of the R and L ligands. Moreover, with the more complex R groups, C_6F_5 or C_6Cl_5, a third component has been found to arise, which involves multicenter electrostatic interactions between the positively charged NO ligand and the negatively charged halo-substituents in the *ortho*-position of the C_6X_5 groups (X = F, Cl). The contribution of each component to the Pt–NO bonding in R_4Pt–NO and $(C_6F_5)_3(L)Pt$–NO compounds seems to be modulated by the electronic and steric effects of the R and L ligands.

Keywords: density functional calculations · metal nitrosyls · platinum · structure elucidation · transition metals

Introduction

The chemistry of transition metal coordination compounds containing the nitrosyl (NO) ligand has seen a tremendous revival since the discovery[1] of NO as an essential biological molecule.[2] More recent focus has been drawn to nitrosyl complexes as drugs that release the neurotransmitter and mammalian bioregulator NO,[3] as model complexes for metal enzymes such as the nitrile hydrase,[4] cytochrome oxidase,[5] and nitrogenase,[6] and as potential waste gas purification catalysts.[7] Catalytic cycles involving alkali[8] and alkaline earth[9] metals have been proposed for the destruction of NO in combustion exhaust gases. The NO ligand can act as diamagnetic, strongly π-accepting NO^+, as the equally diamagnetic NO^-, or as the paramagnetic, neutral NO. As a consequence the specific electronic, structural, and reactivity features of the transition metal nitrosyl complexes have aroused interest since the early days of coordination chemistry. A variety of [M]–NO, or [M]–NO^+ type of complexes, where [M] is a metal fragment, have recently been studied,

[a] Prof. Dr. J. Forniés, Dr. I. Ara, Dipl.-Chem. M. A. García-Monforte, Dr. B. Menjón, Dipl.-Chem. R. M. Sanz-Carrillo, Dr. M. Tomás
Departamento de Química Inorgánica
Instituto de Ciencia de Materiales de Aragón
Facultad de Ciencias, Universidad de Zaragoza-C.S.I.C.
Pza. S. Francisco s/n, 50009 Zaragoza (Spain)
Fax: (+34)976761187
E-mail: forniesj@unizar.es

[b] Prof. Dr. C. A. Tsipis, Dr. A. C. Tsipis
Laboratory of Applied Quantum Chemistry
Faculty of Chemistry
Aristotle University of Thessaloniki
54006 Thessaloniki (Greece)

Supporting information (PDB files for the solid state structures of **2c** and the anion of **4**·0.5 CH_2Cl_2; Figures S1–S6 showing the fully optimized geometries along with the atom-labeling Scheme of complexes **9**–**13**; Table S1 summarizing the natural bond orbital (NBO) and Mulliken population analysis data and Tables S2–S4 showing selected bond lengths and bond angles of complexes **9**–**13**) for this article is available on the WWW under http://www.chemeurj.org/ or from the author.

DOI: 10.1002/chem.200204627

using density functional theory (DFT) at various levels,[10] but surprisingly enough, the number of ab initio studies is very limited[11] and not sufficiently systematic. Timely and important areas of NO chemistry from physical and computational studies to the biological role in living systems have been covered in a recent issue of *Chemical Reviews*.[12] One of the goals of this work is to understand all possible bonding modes of the terminal nitrosyl ligand coordinated to Pt-metal centers in various mononuclear platinum nitrosyl systems and the role of the stabilizing coligands. A salient feature of terminal metal nitrosyl complexes is the geometry of the [M]–NO unit ranging from bent (ca. 120°) to linear (ca. 180°). We had found that the pentachlorophenyl group is a well-behaved ligand allowing a convenient entry to platinum nitrosyl systems. With the synthesis of $[NBu_4][Pt(C_6Cl_5)_4(NO)]$[13] and $[NBu_4][Pt(C_6Cl_5)_2Cl_2(NO)]$[14] we obtained examples of both linear and bent platinum nitrosyl species for a same $\{PtNO\}^8$ electronic configuration. We report now a combined computational and experimental study of perhalophenyl-nitrosyl derivatives of platinum in order to understand the role of the stabilizing coligands in the bonding mode of the [Pt]–NO unit.

Results and Discussion

Synthesis and characterization of the precursors: The series of tris(pentafluorophenyl)platinate(II) derivatives $[NBu_4][Pt(C_6F_5)_3(L)]$ (**1**) [L = CN*t*Bu (**1a**), NC_5H_4Me-4 (**1b**), $PPhMe_2$ (**1c**), PPh_3 (**1d**) and tht (**1e**)], was found appropriate to allow a systematic study of their behaviour against NO^+. Compounds **1d** and **1e** were prepared according to a published method.[15] The new species **1a**, **1b** and **1c** were prepared in good yield as white solids by room temperature reaction of $[NBu_4]_2[Pt(C_6F_5)_3Cl]$ with an equimolar amount of $AgClO_4$ in the presence of the corresponding ligand L [Eq. (1)].

$$[NBu_4]_2[Pt(C_6F_5)_3Cl] + L \xrightarrow[-AgCl,\ -[NBu_4]ClO_4]{+AgClO_4} [NBu_4][Pt(C_6F_5)_3(L)] \quad (\mathbf{1}) \qquad (1)$$

Compounds **1a–c** have been characterized by analytical and spectroscopic methods. The IR spectra (Table 1)[16] show three absorptions assignable to the so-called X-sensitive vibration modes,[17] as expected for a square-planar $[MX_3L]$ species (C_{2v}, IR active $\Gamma_{M\text{-}C}$ fundamentals: $2A_1+B_1$). Each of the ^{19}F NMR spectra (Table 2) shows two sets of C_6F_5 signals corresponding to the chemically inequivalent *trans*- and *trans*-to-L C_6F_5 groups. These signals are easily assignable to each kind of C_6F_5 group because of their 2:1 relative integrated ratio with the exception of the *m*-F and *p*-F signals of **1c**, which appear so intermingled that a reliable assignment is not possible in this case. The $^3J(^{195}Pt,F)$ values lie between 342 and 535 Hz. The CN*t*Bu ligand in **1a** gives rise to an IR absorption at 2187 cm^{-1} assignable to $\nu(C{\equiv}N)$ and to a low-frequency singlet in the ^1H NMR spectrum ($\delta = 1.31$, Me). The ^1H NMR spectrum of **1b** shows a singlet in the aliphatic region ($\delta = 2.15$) due to the *p*-Me group of the NC_5H_4Me-4 ligand together with two signals in the aromatic region ($\delta =$ 8.48 and 6.86) which can be assigned to the *o*-H and *m*-H, respectively, because of the presence of not completely resolved ^{195}Pt satellites in the high-frequency signal [$^3J(^{195}Pt,H) = 25$ Hz]. The ^{31}P NMR spectrum of **1c** shows a single signal at $\delta = -14.7$ with ^{195}Pt satellites [$^1J(^{195}Pt,P) =$ 2568 Hz] due to the $PPhMe_2$ ligand.

Synthesis and characterization of the new five-coordinate Pt-nitrosyl complexes: When the precursors $[NBu_4][Pt(C_6F_5)_3(L)]$ (**1**), L being a typical representative for C-, N-, P- and S-donor ligands, react with an equimolar amount of $NOClO_4$, the colour of the solutions turns reddish brown. From these solutions, the neutral platinum nitrosyl compounds with formula $[Pt(C_6F_5)_3(L)(NO)]$ (**2**) [L = CN*t*Bu (**2a**), NC_5H_4Me-4 (**2b**), $PPhMe_2$ (**2c**), PPh_3 (**2d**) and tht (**2e**)] can be isolated as brown solids in moderate yield [Eq. (2)].

$$[NBu_4][Pt(C_6F_5)(L)] \xrightarrow[-[NBu_4]ClO_4]{+NOClO_4} [Pt(C_6F_5)_3(L)(NO)] \quad (\mathbf{2}) \qquad (2)$$

The ionic compound $[N(PPh_3)_2][Pt(C_6F_5)_4(NO)]$ (**4**) has also been obtained as a brown solid by 1:1 reaction of the homoleptic species $[N(PPh_3)_2]_2[Pt(C_6F_5)_4]$ (**3**) with $NOClO_4$ under similar conditions [Eq. (3)]. Better yields are obtained if the reactions leading to **2** or **4** are carried out under a NO atmosphere.

$$[N(PPh_3)_2][Pt(C_6F_5)_4] \xrightarrow[-[N(PPh_3)_2]ClO_4]{+NOClO_4} [N(PPh_3)_2][Pt(C_6F_5)_4(NO)] \quad (\mathbf{4}) \qquad (3)$$

Table 1. IR data [cm^{-1}].[a]

Compound	ν(NO)[b]	ν(NO)	ν(C–F)	X-sensitive[c]	Other
$[NBu_4][Pt(C_6F_5)_3(CNtBu)]$ (**1a**)	–	–	953	798, 785, 772	2187 (C≡N), 1633, 1607, 1054, 530, 462
$[NBu_4][Pt(C_6F_5)_3(NC_5H_4Me\text{-}4)]$ (**1b**)	–	–	953	801, 786, 771	1628, 1606, 1525, 1055, 500
$[NBu_4][Pt(C_6F_5)_3(PPhMe_2)]$ (**1c**)	–	–	955	801, 794, 772	1672, 1634, 1109, 1056, 909, 839, 696, 494
$[Pt(C_6F_5)_3(CNtBu)(NO)]$ (**2a**)	1820	1832	971	804, 784	2213 (C≡N),[d] 2183 (C≡N),[d] 1639, 1613, 1510, 1065, 533
$[Pt(C_6F_5)_3(NC_5H_4Me\text{-}4)(NO)]$ (**2b**)	1829	1824, 1812	967	811, 786	1634, 1511, 1068, 556
$[Pt(C_6F_5)_3(PPhMe_2)(NO)]$ (**2c**)	1800	1825, 1802	967	795, 782	1639, 1611, 1511, 1109, 1062, 839, 696, 492
$[Pt(C_6F_5)_3(PPh_3)(NO)]$ (**2d**)	1805	1835, 1803	965[e]	802, 786	1639, 1612, 1504, 1069, 756, 740, 699, 531, 511, 498
$[Pt(C_6F_5)_3(tht)(NO)]$ (**2e**)	1801	1842, 1822	964[f]	800, 782	1611, 1540, 1510, 1264, 1062
$[N(PPh_3)_2][Pt(C_6F_5)_4(NO)]$ (**4**)	1808	1820	960[g]	789	1639, 1610, 1502, 1058

[a] Unless otherwise stated IR data were obtained from Nujol mulls. [b] In Et_2O solution. [c] Ref. [17]. [d] A single band is observed at 2197 cm^{-1} in CH_2Cl_2 solution. [e] ν(C–F) = 950 cm^{-1} in the parent species **1d** (see ref. [16]). [f] ν(C–F) = 950 cm^{-1} in the parent species **1e** (see ref. [16]). [g] ν(C–F) = 953 cm^{-1} in the parent species **3**.

Table 2. ^{19}F NMR data in solution (δ values in ppm referred to $CFCl_3$).[a]

Compound	*trans* C_6F_5 groups			*trans*-to-L C_6F_5 group		
	o-F[b]	*m*-F	*p*-F	*o*-F[b]	*m*-F	*p*-F
$[NBu_4][Pt(C_6F_5)_3(CNtBu)]$ (**1a**)	−116.90 (342)	−166.42	−165.36	−117.46 (439)	−167.16	−166.02
$[NBu_4][Pt(C_6F_5)_3(NC_5H_4Me\text{-}4)]$ (**1b**)	−119.07 (412)	−166.05	−168.12[c]	−117.41 (535)	−168.20[c]	−165.85
$[NBu_4][Pt(C_6F_5)_3(PPhMe_2)]$ (**1c**)	−116.25 (412)	−166.0 to −166.6[d]		−116.76 (367)[e]	−166.0 to −166.6[d]	
$[Pt(C_6F_5)_3(CNtBu)(NO)]$ (**2a**)[f]	−116.17 (145), −134.32	−162.2, −162.8	−156.54	−119.71 (372)	−160.98	−158.27
$[Pt(C_6F_5)_3(NC_5H_4Me\text{-}4)(NO)]$ (**2b**)[f]	−118.57, −126.06	−160.56	−156.62	−116.29 (170), −130.27	−162.56	−158.30
$[Pt(C_6F_5)_3(PPhMe_2)(NO)]$ (**2c**)[f]	−112.04, −124.65	−159.8, −160.6	−156.65	−115.42, −130.31	−161.65	−157.81
$[Pt(C_6F_5)_3(PPh_3)(NO)]$ (**2d**)[f]	−108.83, −123.95	−161 to −163[d]	−158.18	−114.74, −132.83	−161 to −163[d]	−158.74
$[Pt(C_6F_5)_3(tht)(NO)]$ (**2e**)[f]	−114.25, −126.34	−159.66, −160.48	−155.85	−116.43, −132.49	−161.70	−157.66
$[N(PPh_3)_2][Pt(C_6F_5)_4(NO)]$ (**4**)[f]	−114.5, −128.3	−164.6	−162.2	–[g]	–[g]	–[g]
$[N(PPh_3)_2][Pt(C_6F_5)_4(NO)]$ (**4**)[h]	−121.4	−165.5	−163.2	–[g]	–[g]	–[g]

[a] Room temperature measurements, unless otherwise stated. [b] Where observed and sufficiently resolved, $^3J(^{195}Pt,F)$ values are given in Hz in parenthesis. [c] These signals appear intermingled with each other. [d] Severe superposition of the signals precludes a reliable assignment. [e] Broad signal. [f] Recorded at −60 °C. [g] N.A. [h] Recorded at 45 °C.

The synthetic procedure can be considered as a Lewis neutralization process in which the platinate moiety acts as the base and the NO^+ cation as the acid. The behaviour of anionic poly(perhalophenyl)platinate derivatives as Lewis bases has been well documented, especially against a variety of metal acidic species such as Ag^I, Hg^{II}, Tl^I, Tl^{III}, Sn^{II} and Pb^{II}.[18]

Compounds **2** and **4** have been characterized by analytical and spectroscopic methods. The IR spectra of **2a** and **4** show single absorptions at $\approx$1820 cm^{-1} both in solution and in the solid state (Table 1), assignable to ν(NO). The fact that **2b**–**e** show two close absorptions in the same region in the solid state can be attributed to lattice effects since, in CH_2Cl_2 solution, single absorptions are also observed. Lattice effects may also be responsible for the two absorptions assignable to ν(C≡N) observed in the IR spectrum of solid **2a**, since they convert into a single band in CH_2Cl_2 solution. High-frequency shifts are observed for the ν(C–F) values in all cases. Although such noticeable shifts in pentafluorophenyl-palladium and -platinum compounds have been associated to changes in the metal oxidation state,[17a] it is also known that ascribing a precise oxidation state to a given metal nitrosyl species is, at least, controversial. It is therefore, that we make no assumption about the oxidation state of the Pt center in compounds **2** and **4** and define them as {PtNO}^{8} species, thus adhering the Enemark and Feltham formalism.[19] On coordination of NO^+ to the square-planar $[Pt(C_6F_5)_3(L)]^-$ units, a lowering in the metal-center local symmetry would be expected ($C_{2v} \rightarrow C_s$ or $C_{2v} \rightarrow C_1$). Regardless of the precise final geometry of **2**, three X-sensitive vibrations would therefore predicted to be IR active as observed in the corresponding parent compounds **1**. However, the IR spectra of **2** show only two such absorptions. From the good quality of the NMR spectra of **2** and **4**, diamagnetism of the samples can be inferred. The ^{1}H NMR spectra of compounds **2** are similar to those of the corresponding parent species **1** with only minor differences in the chemical shifts and the coupling constants. Thus, for instance, the resonance assigned to the *o*-H atoms of the NC_5H_4Me-4 ligand in **2b** ($\delta = 8.52$) shows no ^{195}Pt satellites, while in **1b** ($\delta = 8.48$) were clearly observable [$^3J(^{195}Pt,H) = 25$ Hz]. The ^{31}P NMR spectra of compounds **2c** and **2d** show single resonances at $\delta = -18.4$ [$^1J(^{195}Pt,P) = 2960$ Hz] and 4.9 [$^1J(^{195}Pt,P) = 2027$ Hz], respectively. The ^{19}F NMR spectra of compounds **2** and **4** registered at different temperatures denote the existence of some dynamic processes and will be discussed later.

The molecular structures of **2c** and **4** were determined by single-crystal X-ray diffraction methods (crystallographic data given in Table 3). The structure of the neutral species $[Pt(C_6F_5)_3(PPhMe_2)(NO)]$ (**2c**) is depicted in Figure 1. Selected interatomic distances and angles are given in Table 4. The Pt atom is located in a nearly square pyramidal (*SPY*-5) environment as evidenced by the very small value of the

Table 3. Crystal data and structure refinement for **2c** and **4**·0.5CH_2Cl_2.

	2c	**4**·0.5CH_2Cl_2
formula	$C_{26}H_{11}F_{15}NOPPt$	$C_{60.5}H_{31}ClF_{20}N_2OP_2Pt$
M_r	864.42	1474.34
T [K]	293(2)	200(2)
λ [Å]	0.71073	0.71073
crystal system	monoclinic	triclinic
space group	$P2_1/n$	$P\bar{1}$
a [Å]	10.394(2)	12.117(3)
b [Å]	18.754(2)	13.101(3)
c [Å]	14.759(3)	20.187(5)
α [°]	90	85.76(2)
β [°]	108.21(1)	74.64(2)
γ [°]	90	78.14(2)
V [Å^3]	2732.9(8)	3023.5(13)
Z	4	2
ρ [g cm^{-3}]	2.101	1.618
μ [mm^{-1}]	5.319	2.521
F(000)	1640	1440
diffractometer	Siemens-STOE/AED-2	
2θ range [°]	4–50 ($+h, +k, \pm l$)	4–50 ($\pm h, \pm k, -l$)
refinement method	full-matrix least-squares on F^2	
final R indices [$I > 2\sigma(I)$][a]		
R_1	0.0268	0.0294
wR_2	0.0485	0.0762
R indices (all data)		
R_1	0.0450	0.0375
wR_2	0.0535	0.0787
goodness-of-fit on F^2[b]	1.034	1.002

[a] $R_1 = \Sigma(|F_o| - |F_c|)/\Sigma|F_o|$; $wR_2 = [\Sigma w(F_o^2 - F_c^2)^2/\Sigma w(F_c^2)^2]^{1/2}$; $w = [\sigma^2(F_o^2) + (g_1P)^2 + g_2P]^{-1}$; $P = (1/3)\cdot[\max\{F_o^2, 0\} + 2F_c^2]$. [b] Goodness-of-fit $= [\Sigma w(F_o^2 - F_c^2)^2/(n_{obs} - n_{param})]^{1/2}$.

Table 4. Selected bond lengths [Å] and angles [°] and their estimated standard deviations for **2c**.

Bond lengths			
Pt(1)–N(1)	2.068(7)	C(10)–C(15)	1.372(8)
Pt(1)–C(1)	2.100(6)	C(11)–F(11)	1.358(6)
Pt(1)–C(10)	2.092(6)	C(15)–F(15)	1.366(7)
Pt(1)–C(20)	2.106(6)	C(20)–C(21)	1.382(9)
Pt(1)–P(1)	2.359(2)	C(20)–C(25)	1.376(9)
N(1)–O(1)	1.086(7)	C(21)–F(21)	1.343(8)
C(1)–C(2)	1.373(8)	C(25)–F(25)	1.347(8)
C(1)–C(6)	1.373(8)	P(1)–C(30)	1.808(6)
C(2)–F(2)	1.355(7)	P(1)–C(40)	1.811(6)
C(6)–F(6)	1.366(7)	P(1)–C(50)	1.809(6)
C(10)–C(11)	1.389(8)		
Bond angles			
Pt(1)-N(1)-O(1)	120.1(6)	C(6)-C(1)-C(2)	114.7(6)
N(1)-Pt(1)-C(1)	98.4(2)	Pt(1)-C(10)-C(11)	118.2(4)
N(1)-Pt(1)-C(10)	94.6(2)	Pt(1)-C(10)-C(15)	128.6(5)
N(1)-Pt(1)-C(20)	91.3(3)	C(15)-C(10)-C(11)	113.0(6)
N(1)-Pt(1)-P(1)	97.2(2)	Pt(1)-C(20)-C(21)	125.2(5)
C(1)-Pt(1)-C(10)	166.8(2)	Pt(1)-C(20)-C(25)	119.6(5)
C(1)-Pt(1)-C(20)	85.8(2)	C(25)-C(20)-C(21)	115.1(7)
C(1)-Pt(1)-P(1)	90.3(2)	Pt(1)-P(1)-C(30)	113.0(2)
C(10)-Pt(1)-C(20)	91.3(2)	Pt(1)-P(1)-C(40)	110.2(2)
C(10)-Pt(1)-P(1)	90.7(2)	Pt(1)-P(1)-C(50)	115.0(2)
C(20)-Pt(1)-P(1)	171.1(2)	C(30)-P(1)-C(40)	107.8(3)
Pt(1)-C(1)-C(2)	127.5(5)	C(30)-P(1)-C(50)	106.0(3)
Pt(1)-C(1)-C(6)	117.7(5)	C(40)-P(1)-C(50)	104.3(3)

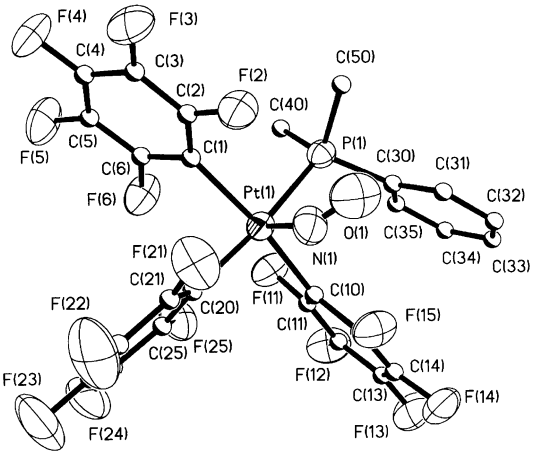

Figure 1. Perspective drawing of **2c** (50 % probability ellipsoids).

angular structural parameter[20] $\tau = 0.072$. The NO ligand is located in the apex of the pyramid and the remaining coordinated ligands define the basal plane. The C_6F_5 groups are tilted with respect to the basal plane with angles between 66° and 78°. The three Pt–C_6F_5 bond lengths in **2c** are virtually identical [between 2.092(6) and 2.106(6) Å] and close to the longest distance found in the related heterodimetallic *SPY*-5 species $[NBu_4][Pt(C_6F_5)_3(tht)\{Ag(PPh_3)\}]$ [Pt–C range: 2.00(1) – 2.10(1) Å].[21] Slightly shorter Pt–C_6F_5 distances were found in the mononuclear square planar derivative $[NBu_4][Pt(C_6F_5)_3(PPh_3)]$ [Pt–C range: 2.04(1) – 2.07(1) Å].[22] The Pt–P bond length in the latter compound [Pt–PPh_3 2.279(3) Å] is also slightly shorter than observed in **2c** [Pt–$PPhMe_2$ 2.359(2) Å]. The Pt-N-O unit is clearly bent [120.1(6)°] towards the $PPhMe_2$ ligand [torsion angle O(1)-N(1)-Pt-P(1) 4°]. This is in agreement with previous theoretical calculations, which predict a bent M-N-O unit for apical *SPY*-5 metal nitrosyl compounds with {MNO}^{8} configuration.[19, 23] Furthermore, bending has been predicted to occur in the plane containing the poorer donors.[23] The most significant structural features related to the Pt-NO coordination in the structurally characterized terminal Pt-nitrosyl complexes are given in Table 5 for comparison.[24, 25]

An ellipsoid drawing of the anion of $[N(PPh_3)_2][Pt(C_6F_5)_4(NO)]$ (**4**) appears in Figure 2. Selected interatomic distances[26] and angles are given in Table 6. The geometry around Pt is best described as *SPY*-5 with the basal plane defined by the four C_6F_5 groups and the apex occupied by the NO ligand ($\tau = 0.072$).[20] All four C_6F_5 groups are tilted (tilt angles between 55 and 79°) and arranged helically around the

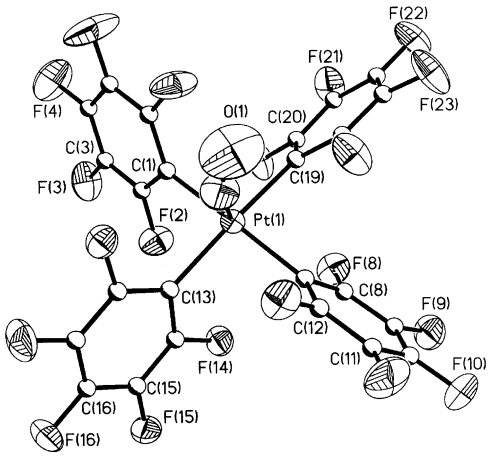

Figure 2. Perspective drawing of the anion of **4** (λ conformation, 50 % probability ellipsoids). The displacement parameters of O(1) are typical for this atom suffering a librational motion. The corresponding N(1) – O(1) distance has been corrected for this effect.[26]

Table 5. Important data relative to the structurally characterized terminal Pt-nitrosyl compounds.

Compound	ν(NO) [cm^{-1}]	Pt coordination environment	Pt – N [Å]	N – O [Å]	Pt-N-O [°]	Ref.
$[NEt_4]_2[\{PtCl_3(NO)\}(\mu\text{-}Cl)(\mu\text{-}NO)\{PtCl_2\}]$		*OC*-6	1.98(6)	1.05(6)	122(5)	[24a]
$[HNC_9H_7]_2[\{PtCl_3(NO)\}_2(\mu\text{-}Cl)_2]$	1750	*OC*-6	2.15[a]	1.18(6)	112.0[a]	[24b]
$[NBu_4][PtCl_2(C_6Cl_5)_2(NO)]$	1797[b]	*SPY*-5	2.054(9)	1.141(14)	119.5(8)	[14]
$[Pt(C_6F_5)_3(PPhMe_2)(NO)]$ (**2c**)	1800[c]	*SPY*-5	2.068(7)	1.086(7)	120.1(6)	this work
$[N(PPh_3)_2][Pt(C_6F_5)_4(NO)]$ (**4**)	1808[c]	*SPY*-5	2.035(4)	1.027(7)	130.2(6)	this work
$[NBu_4][Pt(C_6Cl_5)_4(NO)]$	1791[b]	*SPY*-5	2.22(6)	1.04(9)	180	[13]
NO(g)	1876	–	–	1.15	–	[25]
NO^+(g)	2345	–	–	1.06	–	[25]

[a] Estimated standard deviation not reported. [b] In CH_2Cl_2 solution. [c] In Et_2O solution.

Table 6. Selected bond lengths [Å] and angles [°] and their estimated standard deviations for the anion of **4**·0.5 CH_2Cl_2.

Bond lengths			
Pt(1)–N(1)	2.035(4)	C(8)–F(8)	1.360(5)
Pt(1)–C(1)	2.088(4)	C(12)–F(12)	1.355(5)
Pt(1)–C(7)	2.088(4)	C(13)–C(14)	1.389(6)
Pt(1)–C(13)	2.094(4)	C(13)–C(18)	1.378(6)
Pt(1)–C(19)	2.086(4)	C(14)–F(14)	1.359(5)
C(1)–C(2)	1.380(5)	C(18)–F(18)	1.365(5)
C(1)–C(6)	1.386(6)	C(19)–C(20)	1.376(5)
C(2)–F(2)	1.354(5)	C(19)–C(24)	1.389(6)
C(6)–F(6)	1.355(5)	C(20)–F(20)	1.356(4)
C(7)–C(8)	1.374(6)	C(24)–F(24)	1.364(5)
C(7)–C(12)	1.382(6)	N(1)–O(1)	1.027(7)[a]
Bond angles			
Pt(1)-N(1)-O(1)	130.2(6)	Pt(1)-C(1)-C(6)	126.7(3)
C(1)-Pt(1)-C(7)	168.47(15)	C(2)-C(1)-C(6)	113.1(4)
C(1)-Pt(1)-C(13)	90.03(15)	Pt(1)-C(7)-C(8)	119.6(3)
C(1)-Pt(1)-C(19)	89.58(15)	Pt(1)-C(7)-C(12)	126.7(3)
C(1)-Pt(1)-N(1)	97.10(17)	C(8)-C(7)-C(12)	113.8(4)
C(7)-Pt(1)-C(13)	90.66(15)	Pt(1)-C(13)-C(14)	120.0(3)
C(7)-Pt(1)-C(19)	88.28(15)	Pt(1)-C(13)-C(18)	126.9(3)
C(19)-Pt(1)-N(1)	94.40(18)	C(14)-C(13)-C(18)	113.1(4)
C(13)-Pt(1)-C(19)	172.73(15)	Pt(1)-C(19)-C(20)	121.8(3)
C(13)-Pt(1)-N(1)	90.74(18)	Pt(1)-C(19)-C(24)	124.8(3)
C(7)-Pt(1)-N(1)	96.52(18)	C(20)-C(19)-C(24)	113.4(4)
Pt(1)-C(1)-C(2)	119.9(3)		

[a] The N(1)–O(1) distance given has been corrected for libration.[26]

Pt–N axis with both δ and λ conformations present in the crystal measured (centrosymmetric space group). The Pt–C_6F_5 bond lengths in **4** are very similar [between 2.086(4) and 2.097(4) Å] and are in keeping with the values found in related species of formula $[Pt(C_6F_5)_4(ML_x)]^{n-}$ for which the X-ray crystal structure is known, namely $[NBu_4][Pt(C_6F_5)_4\{Ag(tht)\}]$ [Pt–C range: 2.03(2)–2.09(2) Å],[27] $[NBu_4]_2[\{Pt(C_6F_5)_4\}_2(\mu\text{-Pb})]$ [Pt–C range: 2.05(2)–2.10(2) Å][28] and $[NBu_4]_2[\{Pt(C_6F_5)_4\}_2(\mu\text{-Tl})]$ [Pt–C range: 2.03(2)–2.09(3) Å].[29] The PtNO unit is clearly bent [Pt-N-O 130.2(7)°] and the Pt–N bond length [2.043(5) Å] is similar to that found in **2c** [2.068(7) Å] and in $[NBu_4]_2[PtCl_2(C_6Cl_5)_2(NO)]$ [2.054(9) Å] (Table 5). The N–O bond length [1.027(3) Å] is comparable with that found in ionic $[N{\equiv}O]^+$ (1.06 Å).[25] A comparison between the structures of $[N(PPh_3)_2][Pt(C_6F_5)_4(NO)]$ (**4**) and of the pentachlorophenyl derivative $[NBu_4][Pt(C_6Cl_5)_4(NO)]$ reveals the existence of remarkable differences in the corresponding Pt-N-O units (Table 5) which could not be easily anticipated, especially considering the similar electronic effects traditionally assigned to the C_6F_5 and C_6Cl_5 groups.[30] Thus, bent versus linear NO coordination is observed despite the fact that both species have *SPY*-5 global geometry. They also show noticeably different Pt–N bond lengths [2.043(5) versus 2.22(6) Å]. These structural differences are likely to be related to some differences in the Pt–NO bonding mechanism. In order to ascertain this latter point, we considered it appropriate to undertake a DFT study on various model $[PtR_4(NO)]^-$ (R = H, Me, Cl, CN, C_6F_5 or C_6Cl_5) and $[Pt(C_6F_5)_3(L)(NO)]$ (L = CNMe, PH_3) systems.

The ^{19}F NMR spectrum of **4** at various temperatures (Table 2) is in keeping with a *SPY*-5 geometry for the anion as found in the solid state with at least two different dynamic processes operating in solution. A single *p*-F signal is observed over the whole temperature range studied, meaning that all four C_6F_5 groups are equivalent over that range. Assuming a bent Pt-N-O unit also in solution, this equivalency could be easily achieved by rapid (on the NMR time scale) rotation about the Pt–N axis. In contrast, rotation of the C_6F_5 groups about the corresponding M–C_{ipso} bonds is frequently hindered because of the existence of $d_\pi(M)-p_\pi(C_6F_5)$ interaction, which implies some multiple bond character. The presence of two *o*-F signals in the low temperature spectrum (Figure 3), which coalesce at higher temperatures and eventually merge into a single one at mean frequency, is consistent with the model of hindered rotation of the C_6F_5 groups. The ^{19}F NMR spectra of compounds **2** at different temperatures can be equally well rationalized assuming a dynamic *SPY*-5 structure in solution (Table 2).

Equilibrium geometry, electronic structure and bonding mechanism of the NO ligand in $[R_4Pt(NO)]^-$ (R = H, Me, Cl, CN, C_6F_5, C_6Cl_5), $[Cl_2(C_6Cl_5)_2Pt(NO)]^-$, and $[(C_6F_5)_3(L)Pt(NO)]$ (L = CNMe or PH_3) compounds: The next goal of this work is to determine the details of the electronic structure and, in particular, the nature of the bonding of the nitrosyl ligand in a series of $[R_4Pt(NO)]^-$ (R = H (**5**), Me (**6**), Cl (**7**), CN (**8**), C_6F_5 (**9**), C_6Cl_5 (**10**)) complexes as well as in the mixed-ligand $[Cl_2(C_6Cl_5)_2Pt(NO)]^-$ (**11**), and $[(C_6F_5)_3(L)Pt(NO)]$ (L = CNMe (**12**) or PH_3 (**13**)) compounds. To accomplish this we thought it would be advisable to explore first the effect of the stabilizing co-ligands on the bonding mode of the NO ligand in five-coordinate $[R_4Pt(NO)]^-$ (R = H, Me, Cl or CN) complexes. We selected four ligands exerting different electronic effects, two from the

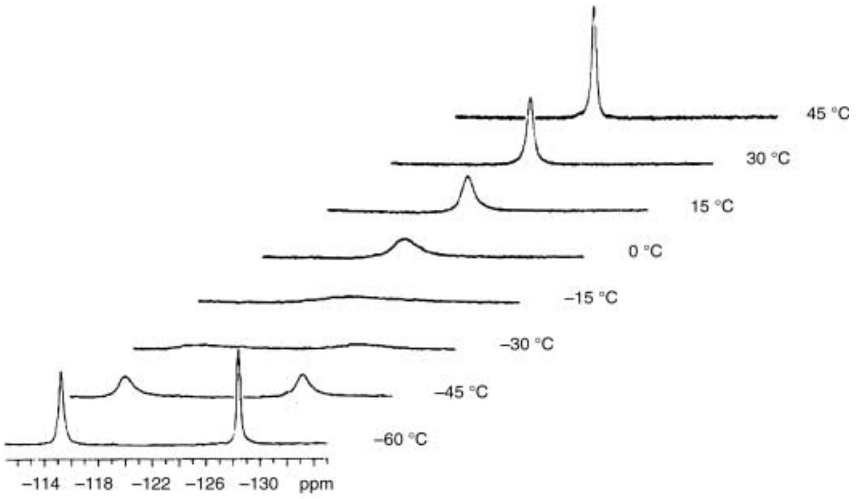

Figure 3. ^{19}F NMR spectrum of **4** (*o*-F region only) registered at various temperatures in [^2H]chloroform.

left, one from the middle and one from the right site of the spectrochemical series. Thus, hydride and methyl are pure σ donors, chloride is a σ donor/π donor, and cyanide a σ donor/π acceptor ligand. In addition, hydride, methyl and cyanide ligands are soft bases, while the chloride ligand is a hard base. Selected geometric parameters for the model $[R_4Pt(NO)]^-$ (R = H, Me, Cl, CN) complexes computed at the B3LYP/SDD level of theory are shown in Figure 4. Interestingly, **5** adopts a distorted TBPY-5 structure involving a

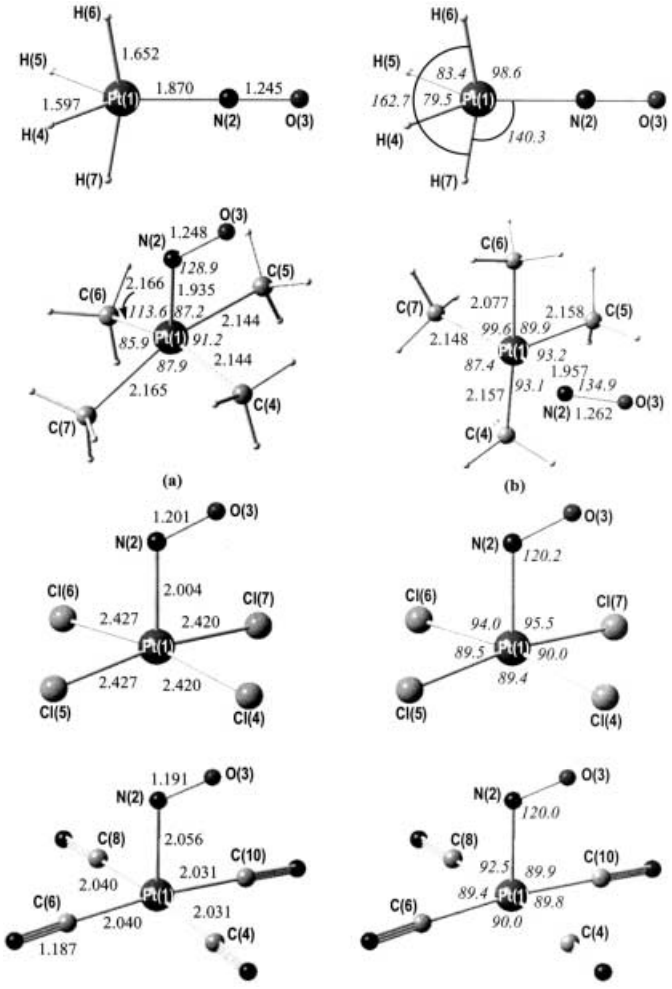

Figure 4. B3LYP-optimized structures of the model $[R_4Pt(NO)]^-$ (R = H, Me, Cl, CN) complexes. For the $[Me_4Pt(NO)]^-$ compound both the apical (a) and basal (b) isomers are given. Bond lengths are in angstroms, and bond angles in degrees.

linearly coordinated NO ligand in the equatorial plane. The H-Pt-H bond angle of the axial Pt–H_{ax} bonds is equal to 162.7°. On the other hand, **6**, **7** and **8** adopt a *SPY*-5 structure with the NO ligand in the apical position coordinated to the Pt central atom in a bent fashion and pointed in the direction of the bisector of one of the R-Pt-R bond angles. The O(3)-N(2)-Pt(1)-C(4), O(3)-N(2)-Pt(1)-Cl(4) and O(3)-N(2)-Pt(1)-C(4) torsion angles in **6**, **7** and **8** are 47.6, 45.5 and 48.5°, respectively. The extent of the bending in **7** and **8** is calculated at similar values of about 120°, whereas in **6** the bending angle is slightly larger (128.9°). The Pt central atom is found 0.15, 0.08, and 0.05 Å above the basal plane of the square pyramidal structures of **6**, **7** and **8**, respectively. The Pt–N bond in **5** is shorter by 0.065, 0.134 and 0.186 Å with respect to the corresponding bond in **6**, **7** and **8**. The N–O bond lengths in **5** and **6** are nearly the same (1.245 versus 1.248 Å), but differ slightly from the N–O bond length in **7** and **8**, being longer by about 0.05 Å. The formation of the $[R_4Pt(NO)]^-$ complexes, viewed as the interaction of NO^+ ligand with the square planar $[R_4Pt]^{2-}$ species are predicted to be exothermic, the computed interaction energies being equal to 353.3, 346.3, 270.7 and 236.3 kcal mol^{-1} for **5**, **6**, **7** and **8**, respectively, at the B3LYP/SDD level of theory. Both the computed interaction energies and the Pt–N bond lengths mirror the different mechanism of bonding of the NO ligand in the linear and bent bonding modes. In the linear bonding mode the Pt–N bond exhibits both a σ and π component (actually it is a partially double Pt–N bond), whereas in the bent bonding mode it is a pure σ bond, in line with the qualitative molecular orbital picture of the bonding modes of the NO ligand. This is further substantiated by the N–O bond length of the coordinated NO ligand, being longer in the linearly than in the bent coordinated NO ligand. Moreover, the observed structural changes of the MNO moiety could be accounted by the electronic effects of the stabilizing co-ligands. Thus, the π acceptor ability of the CN^- ligand is responsible for the withdrawing of electron density from the coordinated NO ligand towards the Pt central atom, thus resulting in the weakening of the Pt–N bond followed by concomitant strengthening of the N–O bond as compared to the σ- and π donor Cl^- ligand. The computed N – O stretching mode for **5**, **6**, **7** and **8** found at 1580, 1507, 1641 and 1686 cm^{-1}, respectively, correlate with the general trend in the N–O bond lengths; this reflects the relative strength of the respective bonds as well as the extent of π-back-donation. Although **6** involves the coordinated NO ligand in a bent-bonding mode similar to that of **7** and **8**, the structural and electronic features of the PtNO moiety are similar to that of **5** as a result of the analogous electronic effects of the methyl and hydride ligands. Looking for an isomer of **6** with a linearly coordinated NO ligand analogous to that found in **5** we located on the PES of **6** another local minimum at almost the same energy corresponding to a square-pyramidal $[Me_4Pt(NO)]^-$ isomer (**6b**) involving the NO ligand in the basal plane of the square-pyramidal structure coordinated again in a bent bonding mode (Figure 4b). In the isomer with the NO ligand in the basal position the bending angle is about 6° larger than the isomer with the NO ligand in the apical position, while both the Pt–N and N–O bonds are longer by 0.022 and 0.034 Å, respectively. It is worth noting that, in spite of the structural differences the computed bond overlap population (bop) values of the Pt–N and N–O bonds in the two isomers are identical. A search for structures involving the linear bonding mode of the NO ligand in a trigonal pyramidal coordination environment of the Pt^{II} center, using the appropriate starting geometries of the optimization process for all $[R_4Pt(NO)]^-$ species revealed the existence of only one minimum corresponding to the aforementioned geometries; both calculations converged to the same geometry.

According to the natural bond orbital (NBO) and Mulliken population analysis (Supporting Information, Table S1) upon

coordination of the NO ligand to Pt central atom there is a strong charge transfer from the Pt central atom to the coordinated NO ligand amounted to 0.97, 0.67, 0.62, 0.44 and 0.49 charge unit of natural charge in **5**, **6a** (apical), **6b**, **7** and **8**, respectively. Note that the computed natural charges on the Pt central atom in $[H_4Pt]^{2-}$, $[Me_4Pt]^{2-}$, $[Cl_4Pt]^{2-}$, and $[(CN)_4Pt]^{2-}$ are -0.59, 0.24, 0.38, and 0.31, respectively. In **5** the linearly bonded NO ligand acquires negative charge, which produces an increase of the N–O bond length with respect to that in free NO molecule. These negative charges are similar to those of the linearly coordinated NO ligand in the square pyramidal $[(CN)_4Fe(NO)]^-$ complex computed at the DFT level of theory.[31] Negatively charged is also the coordinated NO ligand in **6a** and **6b**, isomers as a result of the analogous electronic effects of the hydride and methyl ligands (pure σ donors). On the other hand, the bent coordinated NO ligand in **7** and **8** has a slight positive charge and therefore the N–O bond length is similar to that of the free NO ligand. Generally, the computed bop values follow the trend of the computed Pt–N bond lengths. Surprisingly, though **8** was predicted to be unbound with respect to $[(CN)_4Pt]^{2-}$ and NO asymptotes, the bop value indicates the formation of a weak Pt–NO bond. Interestingly, in all complexes there are two inequivalent Pt–R bond lengths, being more pronounced in the **5** molecule, with the bent PtNO moiety pointed in the direction of the shorter Pt–R bond (Figure 4). To explain the different Pt–R bond lengths we looked for possible bonding multicenter interactions between the N atom of the coordinated NO ligand and the donor atoms of the R ligands. The bop values of 0.024, 0.033 and 0.005 for the N···R interactions for the bonds pointed in the direction of the bent PtNO moiety in **6a**, **6b** and **8**, respectively, strongly suggest the existence of weak interactions. The N···R interactions exist even in the linearly bonded NO ligand in **5** (bop value of 0.008). The interaction of the N atom of the coordinated NO ligand with the other two C donor atoms in **6a** and **6b** isomers is much weaker as it is reflected on the computed bop values of 0.003 and 0.007, respectively. The same is also true for the interaction of the N atom of the coordinated NO ligand with the other two CN^- ligands in **8**, the bop value being only 0.002. However, the bop values of -0.002 and -0.005 for the N···R interactions in **7** are indicative of antibonding N···R interactions. This is substantiated by the nature of the respective molecular orbitals describing the multicenter N···R interactions in the $[R_4Pt(NO)]^-$ compounds. These molecular orbitals, along with the HOMO and LUMO of $[R_4Pt(NO)]^-$ compounds are depicted schematically in Figure 5. Notice the multicenter N···R bonding interactions in HOMO, HOMO-1 and HOMO-2 of **5**, **6a** and **6b** and HOMO-1 and HOMO-2 of **8** and the antibonding orbitals in HOMO-1 and HOMO-2 of **7**.

The LUMO of **5**, **6a**, **6b**, **7**, and **8** at 2.33, 1.96, 2.27, -0.96, and -2.11 eV, respectively, correspond to a π^* MO resulted from the antibonding interaction of an out-of-plane d_π orbital of the Pt atom with the out-of-plane NO π^* orbital. On the other hand, the HOMO of **5**, **6a**, **6b** and **8** at -0.76, -1.41, -0.53 and -5.32 eV, respectively correspond to π^* MO resulted from the antibonding interaction of an in-plane d_π orbital of the Pt atom with the in-plane NO π^* orbital. The

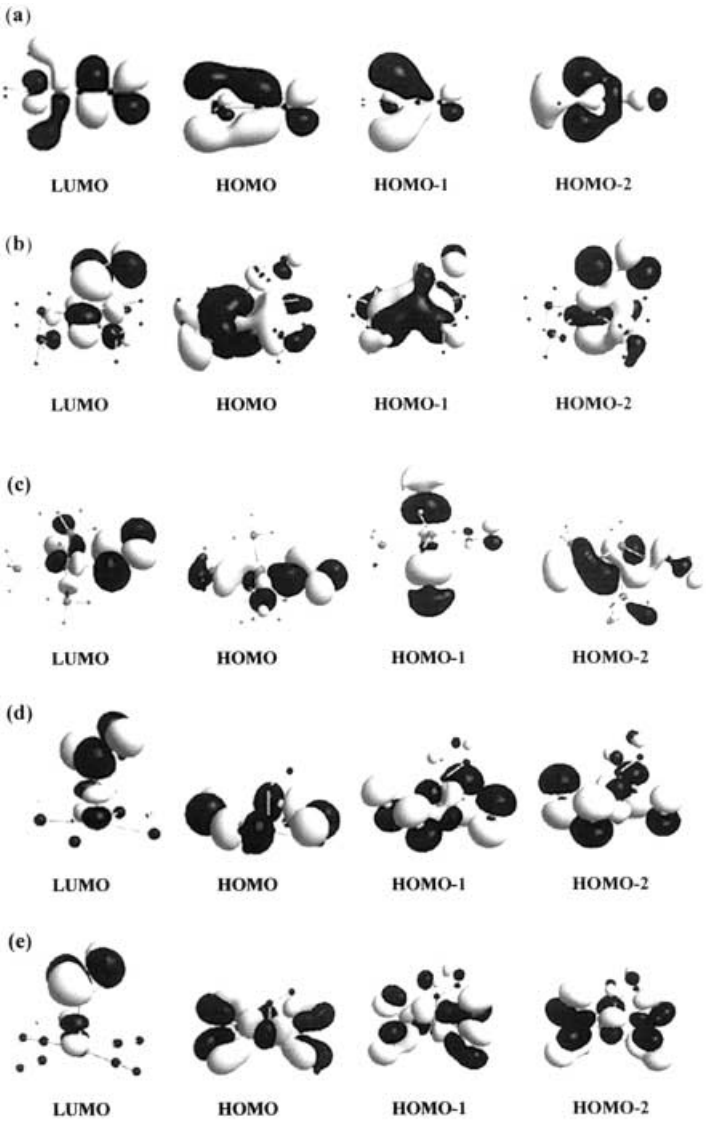

Figure 5. The LUMO, HOMO, HOMO-1 and HOMO-2 of a) $[H_4Pt(NO)]^-$; b) $[Me_4Pt(NO)]^-$ (apical); c) $[Me_4Pt(NO)]^-$ (basal); d) $[Cl_4Pt(NO)]^-$; and e) $[(CN)_4Pt(NO)]^-$.

HOMO of **7** at -3.70 is a non-bonding ligand group orbital resulted from the antibonding interactions of the in-plane *p* AOs of the four chloride ligands. The HOMO–LUMO energy gaps amounted to 3.09, 3.37, 2.80, 3.21 and 2.74 eV for the **5**, **6a**, **6b**, **7** and **8**, respectively, reflect the relative stability of the compounds. Along this line, the multicenter bonding interactions play a critical role in stabilizing the five-coordinate transition metal nitrosyl complexes. Such interactions were also identified previously[32] in the case of 19 valence electron square pyramidal nitrosyl complex $[Fe(pyS_4)NO]$ [pyS_4^{2-} = 2,6-bis-(2-mercaptophenylthiomethyl)pyridine(2–)] with the coordinated NO ligand in a bent bonding mode, respectively, computed at the B3LYP level.

Considering the effect of the electronic properties of the stabilizing co-ligands on the bonding mechanism of the NO ligand in the square pyramidal $[R_4Pt(NO)]^-$ compounds, one would expect, for **9**, **10**, **11**, **12** and **13** involving the more bulky, but electronically equivalent C_6F_5 and C_6Cl_5 ligands, a similar bonding mechanism to that observed in **7** and **8**. The C_6F_5 and

C_6Cl_5 ligands exhibit σ donor, π donor and π acceptor capacity and with respect to electronic effects are closer to the CN^- ligand. In effect in all these complexes the NO ligand is coordinated to the central Pt atom in a bending mode with the extent of the bending calculated at similar values ranging from 118 to 123°. The equilibrium geometries of **9** – **13** fully optimized at the B3LYP/SDD level of theory along with the atom-labeling are shown in the Supporting Information (Figures S1 – S5). Selected bond lengths and angles are also listed in the Supporting Information (Tables S2 – S4). In general terms the computed structures resemble the experimentally determined structures by X-ray crystallography. However, in the case of **10**, the calculations predicted a bent coordination mode of the NO ligand in contrast to the experimentally determined linear coordination mode, a fact, which will be discussed latter on. In contrast to the square pyramidal $[R_4Pt(NO)]^-$ compounds where the coordinated NO ligand is aligned in the direction of the bisector of one of the R-Pt-R bond angles, in **9** and **10** it is aligned in the direction of one of the Pt–C bonds. The computed τ(O-N-Pt-C) torsion angles in **9** and **10** are 7.8 and -0.3°, respectively, with the experimental values being equal to 15.3 and 0.0°. The same is also true for **12** and **13** with the NO ligand aligned in the direction of the Pt–CN and Pt–P bond. The computed τ(O-N-Pt-C) and τ(O-N-Pt-P) torsion angles are equal to -13.0 and -14.9°. In complex **11** the NO ligand is aligned over the Cl-Pt-C bond angle, the computed τ(O-N-Pt-Cl) and τ(O-N-Pt-C) torsion angles being -29.5 and 64.0, respectively, in excellent agreement with the experimental values of -27.6 and 64.7°. The computed Pt–N bond length of **9**, was found to be longer than the experimentally determined one by 0.024 Å. In contrast, the computed Pt–N bond lengths of **11**, **12** and **13** were found to be shorter than the experimentally determined by 0.008, 0.009, and 0.155 Å, respectively. Surprisingly, the experimentally observed elongation of the Pt–NO bond in the linear bonding mode of the NO ligand could not be understood. The experimental value of 2.22(6) Å of the Pt–NO bond length in **10** is too long to correspond even to a very weak Pt – NO bond. Moreover, the computed bop value of -0.041 is indicative of antibonding Pt – NO interactions in **10** with a linearly coordinated NO^+ ligand. We will try to throw light on the bonding mechanism of the NO ligand in these nitrosyl complexes, after discussing first some other structural features of the complexes. The computed Pt–NO bond lengths of **9**, **10**, **11**, **12** and **13** are close to that of model **8** and therefore the Pt – NO interaction is expected to be very weak. This is substantiated by the computed bop values for the Pt–N bond (Table S1, Supporting Information) found in the range of 0.052 – 0.106; these values are lower than that of **8**. The weak Pt – NO interaction, mainly arising from electrostatic interactions, is also reflected on the computed N – O bond lengths of 1.187 – 1.198 Å, which are very close to that of the free NO ligand (1.199 Å). The experimentally determined N – O bond lengths of **9**, **10**, **11** and **2c** are found to be shorter than the computed N – O bond lengths by 0.160, 0.143, 0.057, and 0.104 Å, respectively. Surprisingly, for **9** and **10** the experimental values of the N – O bond lengths seem to be too short, even shorter than the N – O bond length of the free NO^+ species. This strongly suggests that covalent interactions between the NO^+ ligand and the positively charged Pt^{II} central atom are very weak in these complexes thereby a different bonding mechanism might be responsible for the stabilization of the Pt-NO interaction. In effect, the interactions of the NO^+ ligand with the square planar $[(C_6F_5)_4Pt]^{2-}$, $[(C_6Cl_5)_4Pt]^{2-}$, $[Cl_2(C_6Cl_5)_2Pt]^{2-}$, $[(C_6F_5)_3(CNMe)Pt]^-$ and $[(C_6F_5)_3(PPhMe_2)Pt]^-$ fragments is probably stabilized through electrostatic multicenter interactions between the positively charged NO^+ ligand and the negatively charged halo-substituents in the *ortho*-position of the C_6X_5 (X = F, Cl) ligands. The electrostatic nature of the multicenter N···R interactions is verified by the absence of appropriate MOs corresponding to bonding interactions between the respective atoms as in the case of the **5** and **8** model compounds, and by the very small negative bop values indicative of antibonding interactions as well. The interatomic distances for the multicenter electrostatic interactions in **9**, **10**, **11** and **13** are depicted schematically in Figure 6. It can be seen that for all complexes some of the interatomic distances are smaller than the sum of the van der Waals radii of the respective atoms. Notice that the van der Waals radii of N, O, (F)F^-, (Cl)Cl^- and P are 1.392, 1.349, (1.293)1.396, (1.688)1.912, and 1.784 Å, respectively. It should be noted that very recently a series of charge transfer complexes of NO^+ ligand with various aromatic donors involving strong donor/acceptor interactions have been studied experimentally.[33]

Interestingly, as in the case of **6**, **7** and **8**, in **9**, **10**, **11**, **12** and **13** there are also inequivalent Pt – R bond lengths, with the PtNO moiety pointed in the direction of the shorter Pt–R bond. This is due to possible bonding multicenter interactions between the N atom of the coordinated NO ligand and the donor atoms of the R ligands, being substantiated by the computed bop values. Thus, the computed bop values for the N – C_{ipso} interactions are: 0.018, 0.030 and 0.022 in **9**; 0.030 and 0.022 in **10**; 0.020 and 0.030 in **11**; 0.019 and 0.030 in **12**; 0.019 and 0.029 in **13**. Such multicenter bonding interactions exist also in **10** involving a linearly coordinated NO^+ ligand, the computed bop values for the N – C_{ipso} interactions being 0.016. The interatomic distances in **10** involving the NO ligand in a linear bonding mode, depicted schematically in the Supporting Information (Figure S6), are also in support of the multicenter bonding interactions.

Upon coordination of the NO^+ ligand to $[(C_6F_5)_4Pt]^{2-}$, $[(C_6Cl_5)_4Pt]^{2-}$, $[Cl_2(C_6Cl_5)_2Pt]^{2-}$, $[(C_6F_5)_3(CNMe)Pt]^-$ and $[(C_6F_5)_3(PH_3)Pt]^-$ moieties there is a charge transfer from the Pt central atom to the coordinated NO ligand amounted to 0.85, 0.90, 0.97 and 0.88 charge units of natural charge, respectively. The bent coordinated NO ligand in all complexes has a slightly positive charge and therefore the N – O bond length is similar to that of the free NO ligand.

The LUMO of **9**, **10**, **11**, **12**, and **13** at -1.87, -2.10, -1.14, 5.17, and -5.19 eV, respectively, correspond to a π^* MO resulted from the antibonding interaction of an out-of-plane d_π orbital of the Pt atom with the out-of-plane NO π^* orbital (Figure 7a). The HOMO of **9** and **10** at -5.17 and -3.54 eV, respectively, correspond to π^* MO resulted from the antibonding interaction of an in-plane d_π orbital of the Pt atom with the in-plane NO π^* orbital (Figure 7a). The HOMO –

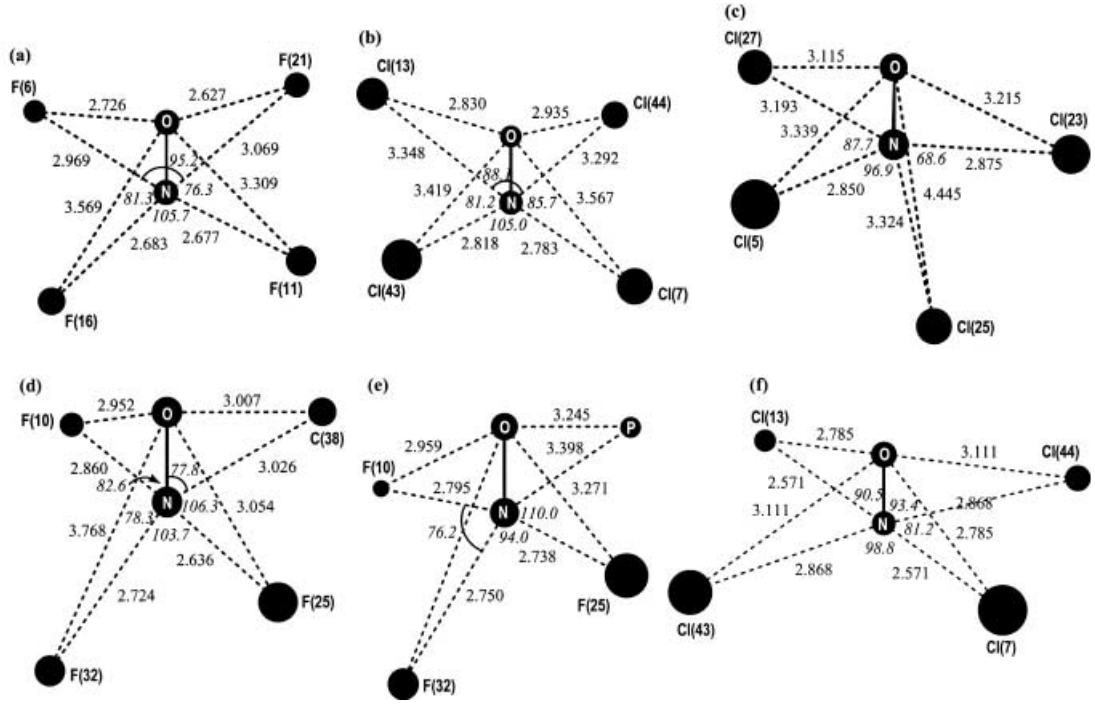

Figure 6. The structural features of the molecular framework describing the multicenter interactions of the NO ligand in a) $[(C_6F_5)_4Pt(NO)]^-$, b) $[(C_6Cl_5)_4Pt(NO)]^-$ c) $[Cl_2(C_6Cl_5)_2Pt(NO)]^-$, d) $[(C_6F_5)_3(CNMe)Pt(NO)]$, e) $[(C_6F_5)_3(PH_3)Pt(NO)]$ and f) $[(C_6Cl_5)_4Pt(NO)]^-$ involving the coordinated NO ligand in a linear bonding mode (experimental structure).

LUMO energy gap amounted to 3.30 and 1.44 eV for **9** and **10** indicates a lower stability of **10**. The HOMO of **11** at −4.28 eV corresponds to an antibonding combination of the d_{yz} AO of the central Pt atom with the p_y AOs of the two chloride ligands (Figure 7b), while the HOMO of **13** at −7.80 and −7.97 eV, respectively, is a π* MO located on the aromatic ring of the C_6F_5 ligand in *trans*-position to the isocyanide and phosphine ligands (Figure 7c). The HOMO–LUMO energy gap amounts to 3.14, 2.63 and 2.78 eV the **11**, **12** and **13**, respectively.

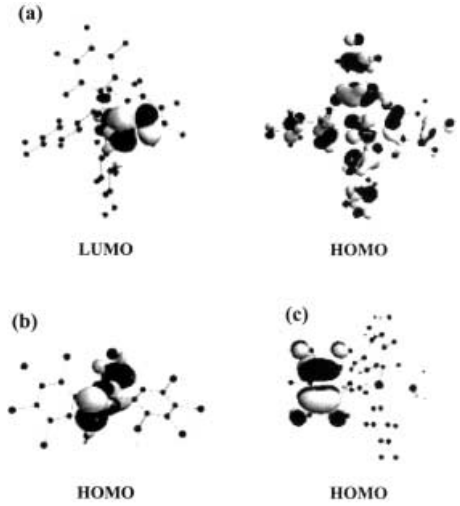

Figure 7. The LUMO and HOMO of a) $[(C_6F_5)_4Pt(NO)]^-$ and the HOMO of b) $[Cl_2(C_6Cl_5)_2Pt(NO)]^-$ and c) $[(C_6F_5)_3(PH_3)Pt(NO)]$ complexes.

Conclusion

A square pyramidal structure has been found for the five-coordinate anions $[Pt(C_6X_5)_4(NO)]^-$ (X = F or Cl). However, the {MNO}[8] unit seems to be very sensitive to the surrounding ligands. Thus, a linear geometry has been found for X = Cl (Pt-N-O 180°), while for X = F it is clearly bent (Pt-N-O 130°).

The bonding mechanism of the nitrosyl ligand coordinated to Pt metal centers in various five-coordinate $[R_4Pt(NO)]^-$ and $[(C_6F_5)_3(L)Pt(NO)]$ complexes has been studied using DFT calculations at the B3LYP level of theory. It was found that the interaction of the NO ligand with the Pt metal centers in these complexes involves three components: i) a direct bonding interaction of the NO ligand with the Pt central atom, ii) multicenter bonding interactions between the N atom of the coordinated NO ligand and the donor atoms of the R or L ligands and iii) multicenter electrostatic interactions between the positively charged NO ligand and the negatively charged halo-substituents in the *ortho*-position of the C_6X_5 (X = F, Cl) ligands. The contribution of each component to the bonding mechanism of the NO ligand with the Pt central atom seems to be modulated by the electronic and steric effects of the ligands R. It can be concluded that the electronic effects of the stabilizing co-ligands in the five-coordinate $[R_4Pt(NO)]^-$ (R = H, Me, Cl, CN, C_6F_5, C_6Cl_5) and $[Pt(C_6F_5)_3(L)(NO)]$ (L = CNMe, PH_3) complexes tune mainly the structural features of the PtNO moiety, but have no effect on the coordination mode (linear versus bent) of the NO ligand. These results point to the possibly important role of the second sphere coordination environment in the stability and chemical behaviour of metal nitrosyls.

Experimental Section

General procedures and materials: Unless otherwise stated, the reactions and manipulations were carried out under purified argon using Schlenk techniques. Solvents were dried by standard methods and distilled prior to use. The starting materials NO,[34] $NOClO_4$,[35] $AgClO_4$,[36] $[N(PPh_3)_2]Cl$,[37] $[NBu_4]_2[Pt(C_6F_5)_3Cl]$,[15] $[NBu_4][Pt(C_6F_5)_3(PPh_3)]$,[38] $[NBu_4][Pt(C_6F_5)_3(tht)]$,[38] and $[NBu_4]_2[Pt(C_6F_5)_4]$,[38] were prepared as described elsewhere. Elemental analyses were carried out with a Perkin – Elmer 2400-Series II microanalyzer. IR spectra of Nujol mulls or CH_2Cl_2 solutions were recorded on a Perkin-Elmer 883 spectrophotometer ($4000-200\ cm^{-1}$). Unless otherwise stated, NMR spectra were recorded at room temperature on [^{2}H]chloroform solutions using a Varian Unity-300 spectrometer: ^{1}H (300 MHz), ^{31}P (121.442 MHz) and ^{19}F (282.231 MHz) chemical shifts are referred to $SiMe_4$, $CFCl_3$ and 85% H_3PO_4 zero values respectively. NMR signals due to the cation are not given. Mass spectra were recorded on a VG-Autospec spectrometer with the standard Cs-ion FAB (acceleration voltage: 35 kV).

Caution: Some of the following synthetic procedures involve working with perchlorate salts. Although in our experience $AgClO_4$, $[N(PPh_3)_2]ClO_4$ and NBu_4ClO_4 are well-behaved materials, it would be advisable to proceed with caution when attempting to repeat those experiments in which these salts are involved because of their potentially explosive nature.[39] $NOClO_4$ is, in turn, known to react violently with, for instance, Me_2CO, Et_2O and EtOH[40] and hence it is advisable not to attempt the reactions involving this material in organic solvents other than CH_2Cl_2 or $CHCl_3$.

Synthesis of $[NBu_4][Pt(C_6F_5)_3(CNtBu)]$ (1a): C*N*tBu (47 μL, 0.41 mmol) and $AgClO_4$ (85 mg, 0.41 mmol) were added to a THF (20 mL) solution of $[NBu_4]_2[Pt(C_6F_5)_3Cl]$ (0.50 g, 0.41 mmol) and the mixture was stirred for 1 h in the dark. A white precipitate formed (AgCl), which was removed by filtration. The filtrate was evaporated to dryness and the resulting residue was treated with Et_2O (20 mL) to give a suspension from which the white solid (NBu_4ClO_4) was removed by filtration. The new filtrate was evaporated to dryness and the residue was extracted in *i*PrOH (5 mL). The addition of a layer of *n*-hexane (20 mL) followed by slow diffusion at $-30\,^\circ C$ caused the crystallization of **1a** as a white solid, which was filtered and vacuum dried (0.20 g, 48%). ^{1}H NMR: $\delta = 1.31$ (s; Me); MS (FAB –): *m*/*z*: 779 $[Pt(C_6F_5)_3(CNtBu)]^-$, 696 $[Pt(C_6F_5)_3]^-$, 510 $[Pt(C_6F_5)(C_6F_4)]^-$; elemental analysis calcd (%) for $C_{39}H_{45}F_{15}N_2Pt$ (1021.86): C 45.85, H 4.4, N 2.7; found C 45.5, H 4.3, N 2.7.

Synthesis of $[NBu_4][Pt(C_6F_5)_3(NC_5H_4Me\text{-}4)]$ (1b): γ-Picoline (40 μL, 0.41 mmol) and $AgClO_4$ (85 mg, 0.41 mmol) were added to a THF (20 mL) solution of $[NBu_4]_2[Pt(C_6F_5)_3Cl]$ (0.50 g, 0.41 mmol) and the mixture was stirred for 1 h in the dark. A white precipitate formed (AgCl), which was removed by filtration. The filtrate was evaporated to dryness and the resulting residue was treated with *i*PrOH (10 mL) giving **1b** as a white solid, which was filtered, washed with *n*-hexane (2×5 mL) and vacuum dried (0.21 g, 50%). ^{1}H NMR: $\delta = 8.48$ [d, $^3J(H,H) = 6.5$ Hz, $^3J(^{195}Pt,H) = 25$ Hz, 2H; *o*-H], 6.86 (d, 2H; *m*-H), 2.15 (s, 3H; Me); MS (FAB –): *m*/*z*: 789 $[Pt(C_6F_5)_3(NC_5H_4Me\text{-}4)]^-$, 696 $[Pt(C_6F_5)_3]^-$, 510 $[Pt(C_6F_5)(C_6F_4)]^-$; elemental analysis calcd (%) for $C_{40}H_{43}F_{15}N_2Pt$ (1031.86): C 46.6, H 4.2, N 2.7; found C 46.7, H 4.4, N 2.5.

Synthesis of $[NBu_4][Pt(C_6F_5)_3(PPhMe_2)]$ (1c): Using the procedure just described for synthesizing **1b**, **1c** was prepared starting from $[NBu_4]_2[Pt(C_6F_5)_3Cl]$ (0.50 g, 0.41 mmol), $AgClO_4$ (85 mg, 0.41 mmol) and $PPhMe_2$ (60 μL, 0.41 mmol). Complex **1c** was obtained as a white solid (0.31 g, 70%). ^{31}P NMR: $\delta = -14.7$ [$^1J(^{195}Pt,P) = 2568$ Hz]; elemental analysis calcd (%) for $C_{42}H_{47}F_{15}NPPt$ (1076.87): C 46.8, H 4.4, N 1.3; found C 46.65, H 4.4, N 1.4.

Synthesis of $[Pt(C_6F_5)_3(CNtBu)(NO)]$ (2a): The addition of $NOClO_4$ (25 mg, 0.20 mmol) to a CH_2Cl_2 (20 mL) solution of **1a** (0.21, 0.20 mmol) caused this colourless solution to immediately turn reddish brown. After 30 min stirring, the solution was evaporated to dryness and the resulting residue was treated with Et_2O (40 mL) to give a suspension from which the white solid (NBu_4ClO_4) was removed by filtration. The new filtrate was evaporated to dryness and treating the residue with *n*-hexane (20 mL) gave **2a** as a brown solid, which was filtered and vacuum dried (0.10 g, 60%). ^{1}H NMR: $\delta = 1.46$ (s); MS (FAB –): *m*/*z*: 779 $[Pt(C_6F_5)_3(CNtBu)]^-$, 696 $[Pt(C_6F_5)_3]^-$, 529 $[Pt(C_6F_5)_2]^-$; elemental analysis calcd (%) for $C_{23}H_9F_{15}N_2OPt$ (809.40): C 34.1, H 1.1, N 3.45; found C 34.8, H 1.5, N 3.3.

Synthesis of $[Pt(C_6F_5)_3(NC_5H_4Me\text{-}4)(NO)]$ (2b): Using the procedure just described for synthesizing **2a**, **2b** was prepared starting from **1b** (0.20 g, 0.19 mmol) and $NOClO_4$ (25 mg, 0.19 mmol). Complex **2b** is obtained as a reddish brown solid (42 mg, 27%). When the synthesis was carried out in an NO atmosphere, the final yield rose up to 53%. ^{1}H NMR: $\delta = 8.52$ [d, $^3J(H,H) = 4.6$ Hz, $^3J(^{195}Pt,H)$ not observed, 2H; *o*-H], 7.46 (d, 2H; *m*-H), 2.57 (s, 3H; Me); MS (FAB –): *m*/*z*: 789 $[Pt(C_6F_5)_3(NC_5H_4Me\text{-}4)]^-$, 696 $[Pt(C_6F_5)_3]^-$; elemental analysis calcd (%) for $C_{24}H_7F_{15}N_2OPt$ (819.40): C 35.2, H 0.9, N 3.4; found C 33.05, H 1.1, N 3.0.

Synthesis of $[Pt(C_6F_5)_3(PPhMe_2)(NO)]$ (2c): Using the procedure just described for synthesizing **2a**, **2c** was prepared starting from **1c** (0.27 g, 0.25 mmol) and $NOClO_4$ (32 mg, 0.25 mmol). Complex **2c** is obtained as a brown solid (65 mg, 30%). ^{1}H NMR: $\delta = 7.5-7.1$ (m, 5H; Ph), 1.9 [d, $^3J(H,H) = 10.8$ Hz, 6H; Me]; ^{31}P NMR: $\delta = -18.4$ [$^1J(^{195}Pt,P) = 2960$ Hz]; MS (FAB –): *m*/*z* 834 $[Pt(C_6F_5)_3(PPhMe_2)]^-$, 696 $[Pt(C_6F_5)_3]^-$, 529 $[Pt(C_6F_5)_2]^-$; elemental analysis calcd (%) for $C_{26}H_{11}F_{15}NOPPt$ (864.42): C 36.1, H 1.3, N 1.6; found C 36.3, H 1.4, N 1.5.

Synthesis of $[Pt(C_6F_5)_3(PPh_3)(NO)]$ (2d): Using the procedure just described for synthesizing **2a**, **2d** was prepared starting from **1d** (0.41 g, 0.34 mmol) and $NOClO_4$ (44 mg, 0.34 mmol). Complex **2d** is obtained as a brown solid (0.23 g, 68%). ^{1}H NMR: $\delta = 7.6-7.1$ (m, Ph); ^{31}P NMR: $\delta = 4.9$ [$^1J(^{195}Pt,P) = 2027$ Hz]; MS (FAB –): *m*/*z*: 958 $[Pt(C_6F_5)_3(PPh_3)]^-$, 696 $[Pt(C_6F_5)_3]^-$, 529 $[Pt(C_6F_5)_2]^-$; elemental analysis calcd (%) for $C_{36}H_{15}F_{15}NOPPt$ (988.56): C 43.7, H 1.5, N 1.4; found C 45.1, H 1.7, N 1.1.

Synthesis of $[Pt(C_6F_5)_3(tht)(NO)]$ (2e): Using the procedure just described for synthesizing **2a**, **2e** was prepared starting from **1e** (0.26 g, 0.25 mmol) and $NOClO_4$ (32 mg, 0.25 mmol). Complex **2e** is obtained as a brown solid (0.12 g, 60%). ^{1}H NMR: $\delta = 3.16$ (m, 4H; α-CH_2), 1.99 (m, 4H; β-CH_2); MS (FAB –): *m*/*z*: 784 $[Pt(C_6F_5)_3(tht)]^-$, 696 $[Pt(C_6F_5)_3]^-$; elemental analysis calcd (%) for $C_{22}H_8F_{15}NOPtS$ (814.44): C 32.5, H 1.0, N 1.7; found C 33.1, H 1.0, N 1.4.

Synthesis of $[N(PPh_3)_2]_2[Pt(C_6F_5)_4]$ (3): Complex **3** was prepared as described for $[NBu_4]_2[Pt(C_6F_5)_4]$, using $[N(PPh_3)_2]Cl$ as the salt of choice instead of NBu_4Br.

Synthesis of $[N(PPh_3)_2][Pt(C_6F_5)_4(NO)]$ (4): $NOClO_4$ (20 mg, 0.15 mmol) was added to a CH_2Cl_2 (20 mL) solution of **3** (0.30 g, 0.15 mmol) and the mixture was stirred for 30 min. The orange solution was evaporated to dryness and the resulting residue was treated with Et_2O (20 mL) to give a suspension from which the white solid ($[N(PPh_3)_2]ClO_4$) was removed by filtration. The reddish filtrate was evaporated to dryness and the residue was extracted in *i*PrOH (3 mL). The addition of a layer of *n*-hexane (20 mL) followed by slow diffusion at $-30\,^\circ C$ caused the crystallization of **4** as a brown solid, which was filtered and vacuum dried (30 mg, 14%). When the synthesis was carried out in an NO atmosphere, the final yield rose up to 47%. MS (FAB –): *m*/*z*: 863 $[Pt(C_6F_5)_4]^-$, 696 $[Pt(C_6F_5)_3]^-$; elemental analysis calcd (%) for $C_{60}H_{30}F_{20}N_2OP_2Pt$ (1431.92): C 50.3, H 2.1, N 1.95; found C 50.9, H 2.5, N 1.6.

X-ray structure determinations: Crystals of **2c** and $\mathbf{4}\cdot 0.5\,CH_2Cl_2$ suitable for X-ray diffraction studies were obtained by slow diffusion of *n*-hexane layers into CH_2Cl_2 solutions of the corresponding powder compounds at $-30\,^\circ C$. Diffracted intensity data were taken from crystals mounted at the end of a glass fiber with epoxy cement. Crystal data and related parameters are given in Table 3. For **2c**, of the 4537 intensity data (other than checks) collected, 3509 unique observations remained after averaging of duplicate and equivalent measurements and deletion of systematic absences (R_{int} 0.0249); of these, 2776 had $I > 2\sigma(I)$; an absorption correction was applied based on azimuthal scan data (max./min. transmission factors = 1.000/0.615). For $\mathbf{4}\cdot 0.5\,CH_2Cl_2$, 11906 intensity data were collected at 200 K by the $\omega/2\theta$ method, from which 10655 unique observations remained after averaging of duplicate and equivalent measurements and deletion of systematic absences (R_{int} 0.0164), of which, 10310 had $I > 2\sigma(I)$; three check reflections measured at regular intervals showed no loss of intensity at the end of data collection; an empirical absorption correction based on azimuthal scan data was applied (max./min. transmission factors = 0.896/0.753). Lorentz and polarization corrections were applied for both structures, which were solved by Patterson and Fourier methods. All refinements were carried out using the program SHELXL-97.[41] All non-hydrogen atoms were assigned anisotropic displacement parameters and refined without positional constraints except as noted below. All hydrogen atoms were constrained to idealized geometries and assigned isotropic

displacement parameters 1.2 times the U_{iso} value of their attached carbon atoms (1.5 times for methyl hydrogen atoms). For the structure of **2c**, a final difference electron density map showed no peaks above 1 e Å^{-3} (max 0.896; largest diff. hole -0.472 e Å^{-3}). For the structure of **4**·0.5 CH_2Cl_2, regions of electron density located at non-bonding distances to the cation were modeled as lattice dichloromethane that was refined in two positions at 0.25 occupancy each so that the stoichiometry of the complex conformed to the given formula. The final difference electron density map showed one peak above 1 e Å^{-3} (max 1.080; largest diff. hole -0.873 e Å^{-3}) located in the solvent area. For both structures, full-matrix least-squares refinement of the models against F^2 converged to final residual indices given in Table 3.

CCDC-198106 and -198107 contain the supplementary crystallographic data for this paper. These data can be obtained free of charge via www.ccdc.cam.ac.uk/conts/retrieving.html (or from the Cambridge Crystallographic Data Centre, 12 Union Road, Cambridge CB21EZ, UK; fax: (+44)1223–336–033; or e-mail: deposit@ccdc.cam.ac.uk).

Computational details: The structural, electronic and energetic properties of all compounds were computed at the Becke's 3-parameter hybrid functional[42] combined with the Lee–Yang–Parr correlation functional[43] abbreviated as B3LYP level of theory, using the SDD basis set that includes Dunning/Huzinaga valence double-zeta on the first row and Stuttgart/Dresden ECP's on the platinum atom.[44] The hybrid B3LYP functional was used, since it gives acceptable results for molecular energies and geometries, as well as proton donation, and hydrogen bonds.[45] In all computations no constraints were imposed on the geometry. Full geometry optimization was performed for each structure using Schlegel's analytical gradient method,[46] and the attainment of the energy minimum was verified by calculating the vibrational frequencies that result in absence of imaginary eigenvalues. All the stationary points have been identified for minimum (number of imaginary frequencies NIMAG = 0) or transition states (NIMAG = 1). All calculations were performed using the GAUSSIAN98 series of programs.[47] Moreover, the qualitative concepts and the graphs derived from Chem3D program suite[48] highlight the basic interactions resulted from the DFT calculations.

Acknowledgements

We thank the Ministerio de Ciencia y Tecnología and FEDER (Project BQU2002-03997-CO2-02). We also thank the Gobierno de Aragón for a grant to M.A.G.-M.

[1] a) F. Murad, *Angew. Chem.* **1999**, *111*, 1976; *Angew. Chem. Int. Ed.* **1999**, *38*, 1856; b) R. F. Furchgott, *Angew. Chem.* **1999**, *111*, 1990; *Angew. Chem. Int. Ed*. **1999**, *38*, 1870; c) L. J. Ignarro, *Angew. Chem.* **1999**, *111*, 2002; *Angew. Chem. Int. Ed.* **1999**, *38*, 1882.

[2] a) M. Feelisch, J. S. Stamler, *Methods in Nitric Oxide Research*, Wiley, Chichester (UK), **1996**; b) L. J. Ignarro, *Nitric Oxide*, Academic Press, Orlando FL, **2000**; c) D. N. R. Rao, A. I. Cederbaum, *Arch. Biochem. Biophys.* **1995**, *321*, 363; d) F. C. Fang, *Nitric Oxide and Infection*, Kluwer Academic/Plenum Publishers, New York, **1997**, Vol. 1 and the following.

[3] a) S. Moncada, R. M. J. Palmer, E. A. Higgs, *Pharmacol. Rev.* **1991**, *43*, 109; b) P. L. Feldman, O. W. Griffith, D. J. Stuehr, *Chem. Eng. News* **1993**, *71*, 26; c) A. R. Butler, D. L. H. Williams, *Chem. Soc. Rev.* **1993**, *22*, 223.

[4] T. Noguchi, J. Honda, T. Nagamune, H. Sasabe, Y. Inoue, I. Endo, *FEBS Lett.* **1995**, *358*, 9.

[5] M. W. J. Cleeter, J. M. Cooper, V. M. Darley-Usmar, S. Moncada, H. V. Scapira, *FEBS Lett.* **1994**, *345*, 50.

[6] a) J. B. Howard, D. C. Rees, *Chem. Rev.* **1996**, *96*, 2965; b) B. K. Burgess, D. J. Lowe, *Chem. Rev.* **1996**, *96*, 2983; c) R. R. Eady, *Chem. Rev.* **1996**, *96*, 3013.

[7] a) V. Zang, R. van Eldik, *Inorg. Chem.* **1990**, *29*, 4462; b) E. K. Pham, S. G. Chang, *Nature* **1994**, *369*, 139.

[8] R. A. Perry, J. A. Miller, *J. Chem. Kinet.* **1996**, *28*, 217.

[9] O. Monticelly, R. Loenders, P. A. Jacobs, J. A. Martens, *Appl. Catal. B: Environ.* **1999**, *21*, 215.

[10] a) C. K. Ruschel, T. M. Nemetz, D. W. Ball, *J. Mol. Struct. (Theochem)* **1996**, *384*, 101; b) C. K. Ruschel, D. W. Ball, *High Temp. Mater. Sci. (Theochem)* **1997**, *37*, 63; c) J. L. C. Thomas, C. W. Jr. Bauschlicher, M. Hall, *J. Phys. Chem. A* **1997**, *101*, 8530; d) C. Blanchet, H. A. Duarte, D. R. Salahub, *J. Chem. Phys.* **1997**, *106*, 8778; e) , M. Ogasawara, D. Huang, W. E. Streib, J. C. Huffman, N. Gallego-Planas, F. Maseras, O. Eisenstein, K. G. Caulton, *J. Am. Chem. Soc.* **1997**, *119*, 8642; f) A. Fiedler, S. Iwata, *J. Chem. Phys* **1998**, *102*, 3618; g) L. Andrews, M. Zhou, D. W. Ball, *J. Phys. Chem. A* **1998**, *102*, 10041; h) G. P. Kushto, M. Zhou, L. E. Andrews, C. W. Jr. Bauschlicher, *J. Phys. Chem. A* **1999**, *103*, 1115; i) L. Zhang, M. Zhou, *Chem. Phys.* **2000**, *256*, 185; j) L. Krim, L. Manceron, M. E. Alikhani, *J. Phys. Chem. A* **1999**, *103*, 2592; k) E. Vayner, D. W. Ball, *J. Mol. Struct. (Theochem)* **2001**, *542*, 149; l) S. Erkoc, *J. Mol. Struct. (Theochem)* **2001**, *574*, 127.

[11] a) C. W. Jr. Bauschlicher, P. S. Bagus, *J. Chem. Phys.* **1984**, *80*, 944; b) H. Basch, *Chem. Phys. Lett.* **1985**, *116*, 58; c) G. W. Smith, E. A. Carter, *J. Phys. Chem.* **1991**, *91*, 2327; d) J. Hrusak, W. Koch, H. Schwarz, *J. Chem. Phys.* **1994**, *101*, 3898.

[12] a) P. Coppens, I. Novozhilova, A. Kovalensky, *Chem. Rev.* **2002**, *102*, 861; b) L. Andrews, A. Citra, *Chem. Rev.* **2002**, *102*, 885; c) J. Mason, L. F. Larkworthy, E. Moore, *Chem. Rev.* **2002**, *102*, 913; d) T. W. Hayton, P. Legzdins, W. B. Sharp, *Chem. Rev.* **2002**, *102*, 935; e) P. C. Ford, I. M., Lorkovic, *Chem. Rev.* **2002**, *102*, 993.

[13] R. Usón, J. Forniés, M. Tomás, B. Menjón, R. Bau, K. Sünkel, E. Kuwabara, *Organometallics* **1986**, *5*, 1576.

[14] J. Forniés, B. Menjón, R. M. Sanz-Carrillo, M. Tomás, *Chem. Ber.* **1994**, *127*, 651.

[15] R. Usón, J. Forniés, F. Martínez, M. Tomás, R. Fandos, *J. Organomet. Chem.* **1984**, *263*, 253.

[16] M. Tomás, Ph. D. Thesis, University of Zaragoza, Zaragoza (Spain), June **1979**.

[17] a) R. Usón, J. Forniés, *Adv. Organomet. Chem*. **1988**, *28*, 219; b) E. Maslowsky, Jr., *Vibrational Spectra of Organometallic Compounds*, Wiley, New York, **1977**, pp. 437–442.

[18] J. Forniés, A. Martín in *Metal Clusters in Chemistry*, *Vol. 1: Molecular Metal Clusters* (Eds.: P. Braunstein, L. A. Oro, P. R. Raithby), Wiley-VCH, Weinheim, **1999**, Section 1.22, pp. 418–443; R. Usón, J. Forniés, *Inorg. Chim. Acta* **1992**, *198–200*, 165; R. Usón, J. Forniés, M. Tomás, *J. Organomet. Chem.* **1988**, *358*, 525.

[19] J. H. Enemark, R. D. Feltham, *Coord. Chem. Rev.* **1974**, *13*, 339.

[20] The angular structural parameter, τ, has been defined as an index of trigonality. It takes continuous values between 0 and 1 ($0 \le \tau \le 1$) with the lower and upper limits denoting ideal *SPY*-5 and *TBPY*-5 geometries, respectively. For the definition and use of this geometric descriptor of five-coordinate molecules see: A. W. Addison, T. N. Rao, J. Reedijk, J. van Rijn, G. C. Verschoor, *J. Chem. Soc. Dalton Trans.* **1984**, 1349; S. Alvarez, M. Llunell, *J. Chem. Soc. Dalton Trans.* **2000**, 3288.

[21] F. A. Cotton, L. R. Falvello, R. Usón, J. Forniés, M. Tomás, J. M. Casas, I. Ara, *Inorg. Chem.* **1987**, *26*, 1366; R. Usón, J. Forniés, M. Tomás, J. M. Casas, F. A. Cotton, L. R. Falvello, *J. Am. Chem. Soc.* **1985**, *107*, 2556.

[22] I. Ara, M. Tomás, *Acta Crystallogr. Sect. C* **1994**, *50*, 375.

[23] R. Hoffmann, M. M. Chen, M. Elian, A. R. Rossi, M. P. Mingos, *Inorg. Chem.* **1974**, *13*, 2666.

[24] a) J. M. Epstein, A. H. White, S. B. Wild, A. C. Willis, *J. Chem. Soc. Dalton Trans.* **1974**, 436; b) T. S. Khodashova, V. S. Sergienko, A. N. Stetsenko, M. A. Porai-Koshits, L. A. Butman, *Zh. Strukt. Khim.* **1974**, *15*, 471.

[25] J. Laane, J. R. Ohlsen in *Progress in Inorganic Chemistry*, *Vol. 27* (Ed.: S. J. Lippard), Wiley, New York, **1980**, pp. 465–513.

[26] M. Nardelli, *J. Appl. Crystallogr.* **1995**, *28*, 659; M. Nardelli, *Comput. Chem.* **1983**, *7*, 95.

[27] R. Usón, J. Forniés, M. Tomás, I. Ara, J. M. Casas, A. Martín, *J. Chem. Soc. Dalton Trans.* **1991**, 2253.

[28] R. Usón, J. Forniés, L. R. Falvello, M. A. Usón, I. Usón, *Inorg. Chem.* **1992**, *31*, 3697.

[29] R. Usón, J. Forniés, M. Tomás, R. Garde, P. J. Alonso, *J. Am. Chem. Soc.* **1995**, *117*, 1837.

[30] W. A. Shepperd, *J. Am. Chem. Soc.* **1970**, *92*, 5419.

[31] J. A. Gómez, D. Guenzburger, *Chem. Phys.* **2000**, *253*, 73.

[32] D. Sellmann, N. Blum, F. W. Heinemann, B. A. Hess, *Chem. Eur. J.* **2001**, *7*, 1874.
[33] a) S. V. Rosokha, J. K. Kochi, *J. Am. Chem. Soc.* **2002**, *124*, 5620; b) S. V. Rosokha, J. K. Kochi, *J. Am. Chem. Soc.* **2001**, *123*, 8985; c) S. M. Hubig, J. K. Kochi, *J. Am. Chem. Soc.* **2001**, *122*, 8279; d) R. Rathore, J. Hecht, J. K. Kochi, *J. Am. Chem. Soc.* **2002**, *124*, 5620; e) R. Rathore, S. V. Lindeman, K. S. S. P. Rao, D. Sun, J. K. Kochi, *Angew. Chem.* **2000**, *112*, 2207; *Angew. Chem. Int. Ed.* **2000**, *39*, 2123; e) R. Rathore, S. V. Lindeman, J. K. Kochi, *Angew. Chem.* **1998**, *110*, 1665; *Angew. Chem. Int. Ed.* **1998**, *37*, 1585.
[34] R. Steudel, P. W. Schenk in *Handbuch der Präparativen Anorganischen Chemie*, *Vol. 1* (Ed.: G. Brauer), 3rd ed., Ferdinand Enke, Stuttgart, **1975**, p. 470 (Method I).
[35] F. Huber, M. Schmeißer in *Handbuch der Präparativen Anorganischen Chemie*, *Vol. 1* (Ed.: G. Brauer), 3rd ed., Ferdinand Enke, Stuttgart, **1975**, p. 329.
[36] N. R. Thompson in *Comprehensive Inorganic Chemistry*, *Vol. 3* (Eds.: J. C. Bailar, H. J. Emeléus, R. Nyholm, A. F. Trotman-Dickenson), Pergamon Press, Oxford (UK), **1973**, p. 109.
[37] J. K. Ruff, W. J. Schlientz, in *Inorganic Syntheses*, *Vol. 15* (Ed.: G. W. Parshall), McGraw-Hill, New York, **1974**, p. 85 – 87.
[38] R. Usón, J. Forniés, F. Martínez, M. Tomás, *J. Chem. Soc. Dalton Trans.* **1980**, 888; see also ref. [16].
[39] W. C. Wolsey, *J. Chem. Ed.* **1973**, *55*, A335.
[40] K. A. Hofmann, A. von Zedtwitz, *Ber. deutsch. Chem. Ges.* **1909**, *42*, 2031.
[41] G. M., Sheldrick, SHELXL 97, *Program for the Refinement of Crystal Structures from Diffraction Data*; University of Göttingen, Göttingen (Germany), **1997**.
[42] a) A. D. Becke, *J. Chem. Phys.* **1992**, *96*, 2155; b) A. D. Becke, *J. Chem. Phys.* **1993**, *98*, 5648.
[43] C. Lee, W. Yang, R. G. Parr, *Phys. Rev.* **1988**, *B37*, 785.
[44] M. Dolg in *Modern Methods and Algorithms of Quantum Chemistry* (Ed.: J. Grotendorst), *Vol. 1*, John von Neumann Institute for Computing, Jülich (Germany), **2000**, pp. 479 – 508.
[45] a) J. B. Nicholas, *Top. Catal.* **1997**, *4*, 157; b) L. A. Curtis, K. Raghavachari, P. C. Redfern, J. A. Pople, *Chem. Phys. Lett.* **1997**, *270*, 419; c) D. M. Smith, B. T. Golding, L. Radom, *J. Am. Chem. Soc.* **1999**, *121*, 9388; d) A. K. Chandra, M. T. Nguyen, *Chem. Phys.* **1998**, *232*, 299; e) J. B. Nicholas, *Top. Catal.* **1999**, *9*, 181; f) R. Arnaud, C. Adamo, M. Cossi, A. Millet, Y. Vallé, V. Barone, *J. Am. Chem. Soc.* **2000**, *122*, 324.
[46] H. B. Schlegel, *J. Comput. Chem.* **1982**, *3*, 214.
[47] *Gaussian 98*, Revision A.7, M. J. Frisch, G. W. Trucks, H. B. Schlegel, G. E. Scusseria, M. A. Robb, J. R. Cheeseman, V. G. Zakrzewski, J. A. Montgomery, R. E. Stratmann, J. C. Burant, S. Dapprich, J. M. Millan, A. D. Daniels, K. N. Kudin, M. C. Strain, O. Farkas, J. Tomasi, V. Barone, M. Cossi, R. Cammi, B. Mennucci, C. Pomelli, C. Adamo, S. Clifford, J. Orchterski, G. A. Petersson, P. Y. Ayala, Q. Cui, K. Morokuma, D K. Malick, A. D. Rabuck, K. Raghavachari, J. B. Foresman, J. Cioslowski, J. V. Ortiz, B. B. Stefanov, G. Liu, A. Liashenko, P. Piskorz, I. Komaroni, R. Gomperts, R. L. Martin, D. J. Fox, T. Keith, M. A. Al-Laham, C. Y. Peng, A. Nanayakkara, C. Gonzalez, M. Challacombe, P. M. Gill, P. Johnson, W. Chen, M. W. Wong, J. L. Andres, M. Head-Gordon, E. S. Replogle, J. A. Pople, Gaussian Inc., Pittsburgh PA, **1998**.
[48] ChemOffice 97 Cambridge Scientific Computing, Inc., 875 Massachusetts Ave., Suite 41, Cambridge, MA 02139-9586 (USA).

Received: November 29, 2002 [F4627]

